INSTITUT DE FRANCE
Académie des sciences

Comptes Rendus

Chimie

Jundong Wang, Lokmane Abdelouahed, Michael Jabbour and Bechara Taouk

Catalytic hydro-deoxygenation of acetic acid, 4-ethylguaiacol, and furfural from bio-oil over Ni_2P/HZSM-5 catalysts

Volume 24, Special Issue S1 (2021), p. 131-147

Published online: 22 September 2021
Issue date: 4 November 2021

https://doi.org/10.5802/crchim.122

Part of Special Issue: Sustainable Biomass Resources for Environmental, Agronomic, Biomaterials and Energy Applications 2

Guest editors: Mejdi Jeguirim (Institut de Science des Matériaux de Mulhouse, France), Salah Jellali (Sultan Qaboos University, Oman) and Besma Khiari (Water Research and Technologies Centre, Tunisia)

Les Comptes Rendus. Chimie *sont membres du*
Centre Mersenne pour l'édition scientifique ouverte
www.centre-mersenne.org
e-ISSN : 1878-1543

Comptes Rendus
Chimie
2021, 24, nº S1, p. 131-147
https://doi.org/10.5802/crchim.122

Sustainable Biomass Resources for Environmental, Agronomic, Biomaterials and Energy Applications 2 / *Ressources de biomasse durables pour des applications environnementales, agronomiques, de biomatériaux et énergétiques 2*

Catalytic hydro-deoxygenation of acetic acid, 4-ethylguaiacol, and furfural from bio-oil over Ni_2P/HZSM-5 catalysts

Jundong Wang [a], Lokmane Abdelouahed [a], Michael Jabbour [a] and Bechara Taouk [*, a]

[a] Normandie Université, INSA Rouen Normandie, UNIROUEN, LSPC-Laboratoire de Sécurité des Procédés Chimiques, 685 Avenue de l'Université, 76801 Saint-Étienne-du-Rouvray, France

E-mails: jundong.wang@insa-rouen.fr (J. Wang), lokmane.abdelouahed@insa-rouen.fr (L. Abdelouahed), michael.jabbour@univ-rouen.fr (M. Jabbour), bechara.taouk@insa-rouen.fr (B. Taouk)

Abstract. In this paper, catalytic hydro-deoxygenation (HDO) of bio-oil's model molecules (acetic acid, 4-ethylguaiacol, and furfural) using Ni_2P/HZSM-5 catalyst was carried out to better identify the products and make the modeling work of HDO process more reliable. Results showed that low temperatures favored the formation of acetaldehyde and acetone during acetic acid HDO, but disfavored the formation of aromatic hydrocarbons. Acetone was produced via the self-ketonization reaction of acetic acid. In most cases of 4-ethylguaiacol HDO, phenol, cresol, and 2, 4-dimethylphenol were the primary products. For furfural HDO, the major furan and CO products proved that the direct decarbonylation of furfural was the main reaction. Accordingly, the main pathways of acetic acid, 4-ethylguaiacol, and furfural HDO were proposed, which could provide significant guidance for the upgrading of crude bio-oil.

Keywords. Hydro-deoxygenation, Acetic acid, 4-Ethylguaiacol, Furfural, Aromatic hydrocarbons, Ni_2P/HZSM-5.

Available online 22nd September 2021

1. Introduction

Bio-oil from fast pyrolysis of biomass contains abundantly soluble and oxygenated organics such as carboxylic acids, guaiacols and aldehydes etc. [1–4], which result in strong acidity, high viscosity, low calorific value and complex composition of bio-oil [5–8]. For this reason, bio-oil needs to be upgraded (via esterification, aldol condensation, ketonization, cracking, and hydro-deoxygenation (HDO)) before it can be commercially applied [9]. Considering the difficulty in understanding routes of upgrading bio-oil, many of studies were concentrated on catalytic HDO of model molecules of bio-oil to obtain commercial biofuels and chemicals [10–12]. Recently,

* Corresponding author.

nickel phosphide supported on acid solids (Al_2O_3, HZSM-5, etc.) as catalysts for HDO attracted researcher's attention since acid supports can promote synergic interactions between the metal active phase and their intrinsic acid sites [13–15]. Furthermore, the use of acid supports also favored sequential hydrogenation–dehydration–hydrogenation reactions in HDO of molecules [16,17].

Noteworthy, HDO studies of carboxylic acids, guaiacols and aldehydes are mainly focused on nickel catalysts with acid solids, but fewer works use nickel phosphide catalysts with acidic supports. For instance, Chen and Falconer [18] studied the HDO of formic acid via temperature-programmed reaction (TPR) using a Ni/Al_2O_3 and found a total conversion of formic acid at 475 °C and high exposure (520 μmol/g catalyst). Results showed that CO was the main product followed by CO_2 and a small amount of CH_4. Similarly, Peng *et al.* [19] explored the HDO conversion of palmitic acid with a Ni/ZrO_2 catalyst. The deoxygenation mechanism indicated hexadecanal and 1-hexadecanol were the initial products and then undergo decarbonylation to produce *n*-pentadecane and CO.

The HDO of another important family of bio-oil products, the guaiacols, has also been studied. Broglia *et al.* [20] performed experiments on guaiacol HDO using Ni/alumina-silica catalysts with varying Ni and silica amount. High conversions of guaiacol were achieved (up to 84%) in a very short time scale (1 h) and, generally, methylguaiacol and phenol were the primary products at 300 °C under H_2 (50 bar). Zhang *et al.* [11] studied the catalytic HDO of guaiacol using a series of high-loading nickel phosphide catalysts supported on SiO_2–TiO_2. Cyclohexane, cyclohexanol, and 2-methoxycyclohexanol are the main products over all of these catalysts from 200 to 260 °C. In addition, Oyama *et al.* [21] investigated the guaiacol HDO using Ni_2P/ASA, Ni_2P/FCC, Ni_2P/ZSM-5 catalysts. As a whole, the dominant products were cresol and phenol. Especially, the effect of contact time indicated that the main pathway on Ni_2P/ASA was the conversion of guaiacol to the catechol as primary intermediate followed by dehydroxylation to phenol. Recently, Li *et al.* [22] studied the HDO of guaiacol on Ni/HZSM-5 catalysts and reported that a conversion rate of 74.8% and a selectivity of 87.1% for cyclohexane were achieved. Also, it was discovered that mesopores and strong metal-support interaction promoted the conversion of guaiacol and the hydrogenation of guaiacol. In another article, the HDO of guaiacol over Ni/γ-Al_2O_3 was carried out by Tran *et al.* [23]. Results showed that 96.88% guaiacol conversion and 58.98% of 1,2-dimethoxybenzene production were obtained over 10 wt% Ni/Al_2O_3 catalyst calcined at 450 °C. At the same time, it has been observed that guaiacols lead to easy coke formation [24], which results in obstacles in upgrading of bio-oil.

Besides, carboxylic acids and guaiacols, aldehydes (like furfural) are also one of the numerous families of pyrolysis oil components. Zhang *et al.* [25] investigated a one-pot hydrogenation/dehydration conversion of furfural using Ni/SiO_2–Al_2O_3 bifunctional catalysts in a batch reactor and found a high selectivity to pentane and a conversion of 62.99% of furfural. In the study of HDO of *n*-hexane-extracted pyrolysis oil, Zhao and Lercher [26] found that furfural underwent HDO/hydrolysis to form *n*-pentane (64%) and tetrahydropyran (36%) over a Ni/HZSM-5 catalyst at 250 °C under 5 MPa H_2 for 2 h. In addition, Wang *et al.* [27] studied the in situ HDO of furfural in aqueous solution over Ni/Al_2O_3 catalysts under 1 MPa N_2. Results showed that high temperature and amount of Ni loading facilitated the conversion of furfural and a total yield above 85% for furan and 2-methylfuran was reached at 260 °C and at the methanol-to-water ratio of 2:1. More recently, Lan *et al.* [28] explored furfural HDO using SiO_2-supported nickel phosphide catalysts. It was found that the improvement of P content on the catalysts weakens the furan-ring/catalyst interaction, which led to a decreasing activity of ring-opening and ring-hydrogenation reaction.

In this background, this work is dedicated to easily understanding the HDO mechanism of bio-oil by studying the HDO of various model molecules over Ni_2P/HZSM-5 catalysts. Here, acetic acid, 4-ethylguaiacol, and furfural were selected as model molecules of bio-oil due to their abundance in pyrolysis oil [29]. The catalysts were already selected for their performance demonstrated in our previous study of acetone HDO [30], and characterized through the N_2 adsorption/desorption (BET specific surface area and pore size calculation), Inductively Coupled Plasma-Optical Emission Spectrometry (ICP-OES) elemental analysis, X-ray Powder Diffraction (XRD), pyridine adsorption by Fourier

Transform Infrared Spectroscopy (FT-IR), and H_2-TPR using Differential Scanning Calorimetry (DSC). Then, various parameters were examined, such as amount of supported phase, temperature and pressure. An in-depth characterization of liquid and gas products of model molecules HDO was performed. Probable HDO reaction routes for the conversion of the aforementioned molecules were proposed, which provide significant guidance for the selective preparation of liquid fuels and high-value chemicals from bio-oil.

2. Materials and methods

2.1. *Materials*

HZSM-5 (Si/Al ratio 38) was provided by ACS Material LLC in the form of pellets having a diameter of 3 mm and an average length of 10 mm. $(NH_4)_2HPO_4$ (AR, ≥99.0%) was bought from VWR Chemicals. $Ni(NO_3)_2 \cdot 6H_2O$ (AR, 99.9985%) was purchased from Alfa Aesar. HNO_3 (PrimarPlus, trace analysis grade, 70%), acetic acid (analytical reagent grade, ≥99.7%), and isopropanol (IP) (GC analysis grade) were supplied by Fisher Scientific. Furfural (AR, 99%) and 4-ethylguaiacol (AR, ≥98%) were acquired from Sigma-Aldrich. Nonane (AR, 99%) was obtained from Prolabo.

2.2. *Preparation and characterization of the catalysts*

The Ni_2P/HZSM-5 catalysts were prepared by the incipient wetness impregnation method as a first step and temperature-programmed reduction (TPR) as the second step [30]. Here, the support HZSM-5 was first ground and sieved to 0.35–0.6 mm particle size before loading the active phase. The specific preparation process and the characterization results of Ni_2P/HZSM-5 catalysts by N_2 adsorption/desorption (BET surface), ICP-OES elemental analysis, and XRD can be found in our previous work [30]. In addition, the acidity of the catalysts was characterized by FT-IR (Spectrum BX, Perkin Elmer) at different pyridine desorption temperatures (100, 150, 275, and 400 °C) after pyridine adsorption and could be found in the Supplementary materials (Figure S1). The samples of the catalysts were saturated with a small amount of pyridine vapor. Prior to the pyridine adsorption, all the samples were dried at 200 °C for 2 h. The H_2-TPR of the Ni_2P/HZSM-5 catalysts' precursors (not reduced) was performed using a DSC (SENSYS-EVO) instrument with a reduction temperature range from 100 to 600 °C and a total gas flow rate of 30 mL/min (5 vol% of H_2 in N_2).

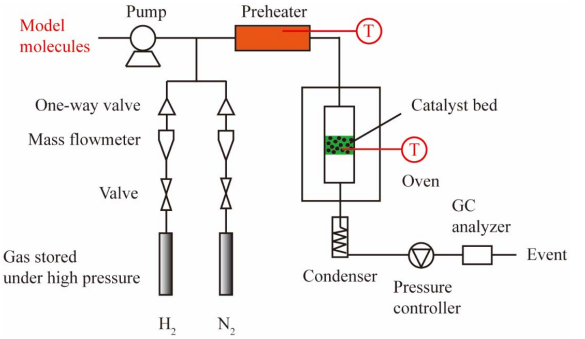

Figure 1. Scheme of continuous fixed-bed reactor.

2.3. *Catalytic activity tests*

2.3.1. *Activity test in setup*

The HDO reaction of acetic acid, 4-ethylguaiacol and furfural were performed in a continuous fixed-bed reactor. The experimental setup can be seen in Figure 1, and most of the operation conditions are the same as our previous study [30]. Here, the liquid reagent, acetic acid, 4-ethylguaiacol or furfural was vaporized in a preheater at a temperature of 150 °C, 260 °C or 200 °C, respectively. The total pressure increased to the desired value of 0.5 MPa or 2 MPa for acetic acid HDO and 0.5 MPa or 3 MPa for 4-ethylguaiacol or furfural HDO, and the temperature went to the designed value of 300–500 °C once the catalysts' reduction process was completed at 450 °C and 0.1 MPa of H_2.

2.3.2. *Products analysis*

Liquid and gas compounds. The analysis of the liquid products was carried out using two different gas chromatographs equipped with the same medium polarity VF-1701-ms column (60 m × 0.25 mm × 0.25 μm film thickness) with two types of detector: mass spectrometer (GC-MS) (Clarus 580/SQ8S) system for identification and flame ionization detector (GC-FID) to quantify the amounts of compounds

in liquid products. Isopropanol was used as the solvent to better analyze the liquid products in GC. Besides, the non-condensable products were gathered in a sampling bag and were then analyzed off-line using a Clarus 580 GC instrument from Perkin Elmer equipped with two detectors, a thermal conductivity (TCD) and a flame ionization detector (FID). The detailed analytical method of products was described in our previous work [30]. The level of experimental error was 2%, which was calculated by experiments repeated thrice.

In order to analyze the experimental results and to better understand the evolution of each model molecule, the conversion rate, selectivity, degree of deoxygenation (DOD), and mass yield were used. The expression of each term is given in the following:

The feedstock conversion X (%) is defined as:

$$X\ (\%) = \frac{n_{\text{feed}^{\text{in}}} - n_{\text{feed}^{\text{out}}}}{n_{\text{feed}^{\text{in}}}} \times 100\% \tag{1}$$

$n_{\text{feed}^{\text{in}}}$: the amount of feedstock injected, mol.
$n_{\text{feed}^{\text{out}}}$: the amount of feedstock in the liquid products, mol.

The selectivity [31] Sel_i (%) of the product chemicals was defined as:

$$\text{Sel}_i\ (\%) = \frac{\text{Carbon number}_i \times n_i}{\text{Carbon number}_{\text{feed}} \times n_{\text{feed}^{\text{converted}}}} \times 100\% \tag{2}$$

Carbon number_i: the number of carbon atoms in the molecular formula of product i, e.g. C_3H_6O, $n_i = 3$.

n_i: the amount of product i, mol.

$n_{\text{feed}^{\text{converted}}}$: the amount of feedstock converted, mol.

The DOD (%) was calculated according to the following equation:

$$\text{DOD}\ (\%) = 1 - \frac{\text{mass of O in liquid products}}{\text{mass of O in feed}_{\text{inlet}}} \times 100\% \tag{3}$$

mass of oxygen in liquid products: the total weight of oxygen in the liquid products (except for water), g.

mass of oxygen in $\text{feed}_{\text{inlet}}$: the total weight of oxygen in feedstock injected, g.

The yield Y_i (%) of chemicals of the products (liquid, gas, and water) was determined using the formula:

$$Y_i\ (\%) = \frac{\text{Mass of product}_i}{\text{Mass of feed}} \times 100\% \tag{4}$$

Mass of product_i is the mass of product i, e.g. mass of H_2O, $i = H_2O$.

3. Results and discussion

3.1. *Catalysts' characterization*

3.1.1. *N_2 adsorption/desorption*

The nitrogen adsorption–desorption isotherms for the catalyst samples are illustrated in Figure 2(A). It can be seen that both the 5% and 10% Ni_2P/HZSM-5 catalysts basically show a combination of IUPAC types I and IV isotherms with a typical type H4 of hysteresis loop. Hence, it can be said that these samples exhibited the co-existence of microporous and mesoporous structures: the extensive adsorption observed below relative pressures ($P/P_0 < 0.2$) is characteristic of microporous structures, while intermediate relative pressures are attributed to mesoporous structures. Type H4 hysteresis is generally associated with narrow slit pores [32].

The pore size distribution of Ni_2P/HZSM-5 catalysts was shown in Figure 2(B). It can be seen that Ni_2P/HZSM-5 catalysts possess a majority of mesoporous distribution from 3 nm to 18 nm and a pinch of the microporous distribution below 2 nm. A higher mesoporous contribution for 5% Ni_2P/HZSM-5 than the case of 10% Ni_2P/HZSM-5 was observed. This can be probably attributed to the smaller Ni_2P phase particles and lower Ni_2P content on the 5% Ni_2P/HZSM-5 compared to the 10% Ni_2P/HZSM-5 catalyst.

3.1.2. *H_2-TPR characterization using differential scanning calorimetry (DSC)*

The H_2-TPR (DSC) of the Ni_2P/HZSM-5 catalysts' precursors with a reduction temperature range from 100 °C to 600 °C can be applied to study the formation process of the Ni_2P active phase. As shown in Figure 3, a small peak was found between 250 °C–300 °C for 5% Ni_2P/HZSM-5 precursor, indicating that some intermediates (for example, $Ni_xP_yO_z$ species) existed during this stage. No peak was observed during this stage in the case of 10% Ni_2P/HZSM-5 precursor. This was probably because the higher Ni and P content formed bigger particles of active phase on the internal surface of pores and surface of 10% Ni_2P/HZSM-5 than 5% Ni_2P/HZSM-5 catalyst and thus prevented the internal $Ni_xP_yO_z$ intermediates from being transformed. The further transformation of intermediates to Ni_2P via the reduction of Ni_xO_y and phosphorus species was associated with the presence of a broad peak at

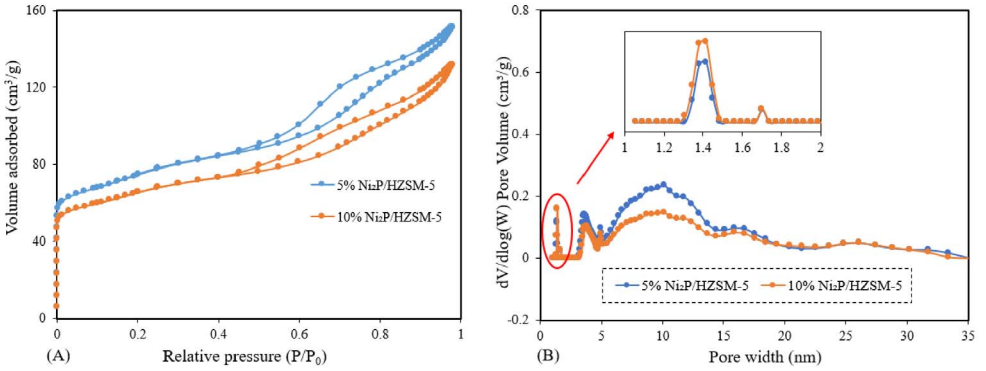

Figure 2. N_2 adsorption/desorption of Ni_2P/HZSM-5 catalysts: (A) isotherms; (B) pore size distributions.

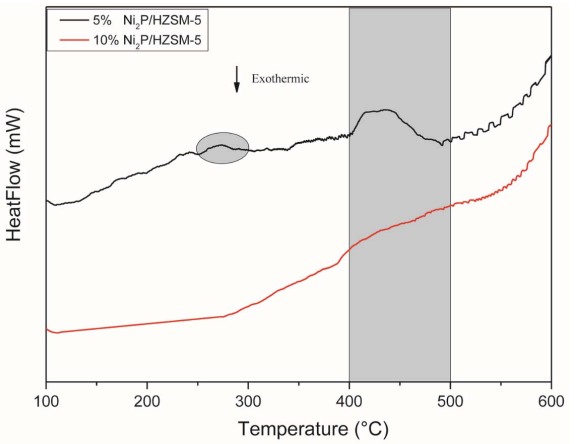

Figure 3. H_2-TPR (DSC) profiles of catalysts' precursors.

an onset temperature around 400 °C. This peak for 5% Ni_2P/HZSM-5 was narrower than the case of 10% Ni_2P/HZSM-5, which also indicated that the intermediates are easier to be reduced. In the literature, Oyama *et al.* also reported almost the same reduction peak of NiO species in the H_2-TPR result of Ni_2P/ASA precursor [21], and Chen *et al.* reported a higher onset reduction temperature around 500 °C of oxidized nickel species and phosphorus species (such as PO_4^{3-}, $P_2O_7^{4-}$, and $(PO_3^-)_n$) to form Ni_2P phase [33].

3.2. *HDO of acetic acid*

To get a liquid product with a low oxygen content, high yield of liquid phase is important and interesting. First of all, HDO of acetic acid using both the 5% and 10% Ni_2P/HZSM-5 catalysts was carried out. The specific results were presented in Supplementary materials (Table S1 and Figure S2). In summary, both the catalysts exhibited an excellent catalytic activity for HDO reaction, and their similar behavior was observed. Subsequently, the 5% Ni_2P/HZSM-5 catalyst was selected for further study.

3.2.1. *Effect of temperature and pressure*

Conversion rate, DOD, and yield. Table 1 showed the effect of temperature and pressure on the conversion rate, DOD, and yield (liquid, gas, and H_2O) of acetic acid HDO. The results exhibited a significantly higher conversion rate (97%) and DOD (96%) at 450 °C than at 350 °C, suggesting that temperature had a relevant effect on the catalytic activity of Ni_2P/HZSM-5. The maximum yield of 50% for gas products was obtained at 450 °C accompanied by the minimum yield of liquid products (28%, H_2O free). This evolution can be attributed to a notable increase in the hydrogenolysis of C–C bonds for acetic acid followed by dehydration and hydrogenation reactions to give more gas products, especially, CO and CO_2. In a previous study, Badari *et al.* [34] found similar results during acetic acid HDO using a Ni/SiO_2 catalyst, namely, that this catalyst favored the C–C bond hydrogenolysis to form lighter gaseous products. Concerning the water content, it first increased, and then decreased when the temperature increased from 350 °C to 450 °C, suggesting that the main reaction of acetic acid HDO at a medium temperature is dehydration.

Selectivity in the liquid phase. The selectivity of major products for acetic acid HDO by varying the

Table 1. Effect of temperature and pressure on acetic acid HDO

Item	Conditions[a]			
	0.5 MPa 350 °C	0.5 MPa 400 °C	0.5 MPa 450 °C	2.0 MPa 350 °C
Conversion rate & DOD (wt%)				
$X_{\text{Acetic acid}}$	61	80	97	69
DOD	59	77	96	68
Yield of products (wt%)				
$Y_{\text{Lip. (free water)}}$	43	33	28	41
Y_{Gas}	40	41	50	45
Y_{H_2O}	17	26	22	14

[a] Fixed conditions: 0.43 g 5% Ni_2P/HZSM-5 catalyst, 0.05 mL/min of acetic acid, H_2: 40 mL/min, N_2: 10 mL/min, 90 min.

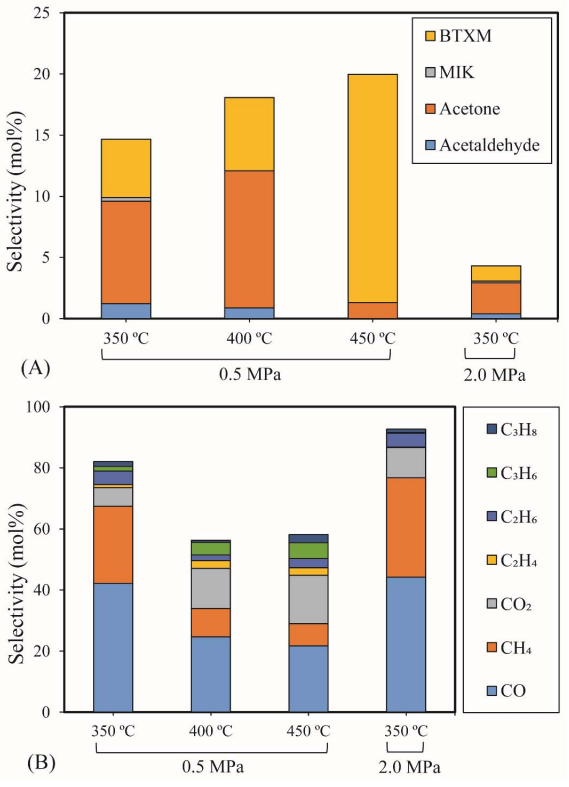

Figure 4. The influence of temperature and pressure on acetic acid HDO (0.43 g 5% Ni_2P/HZSM-5, 0.05 mL/min acetic acid, 40 mL/min H_2, 10 mL/min N_2, reaction time: 90 min): (A) Selectivity of major liquid products; (B) Selectivity of gas products.

temperature and pressure is shown in Figure 4(A). Details of the chemicals identified in the liquid phase can be seen in Supplementary materials (Table S2). The results exhibited a significantly increasing trend in the selectivity of BTXM (benzene, toluene, xylene, and mesitylene) from around 5% to 19% when the temperature increased from 350 °C to 450 °C. In another work, Bej and Thompson [35] reported that mesitylene was formed via aldol condensation between mesityl oxide (MO) and acetone during the investigation of acetone condensation over molybdenum nitride and carbide catalysts. Gamman *et al.* [36] also proposed the same reaction route during the synthesis of methyl isobutyl ketone (MIK) over $Pd/MgO/SiO_2$. On the other hand, MO was not detected in our work, which can be explained by the fact that the reaction from MO to MIK is spontaneous (enthalpy: $\Delta H_{400\,K}$ (kcal/mol) = −14.5; Gibbs free energy: $\Delta G_{400\,K}$ (kcal/mol) = −12.1) [36,37]. Here, it can thus be speculated that the formation of BTXM can be caused by a further aldol condensation between mesityl oxide (MO) and acetone, followed by dehydration, hydrogenation, and isomerization.

Acetone was identified as the main product below 400 °C due to the self-ketonization reaction of acetic acid. This reaction was also observed in the catalytic upgrading of carboxylic acids by Huo *et al.* [38]. The linear MIK was probably obtained at 350 °C through an aldol condensation reaction of acetone [39]. These results indicate that high temperature promotes the condensation reaction to form dimers and trimers. Above 400 °C, the selectivity of acetone decreased

sharply from 11% to 1%, which can be attributed to the conversion of acetone to aromatic hydrocarbons [40]. In addition, acetaldehyde was observed at low temperatures (350 °C and 400 °C) owing to the reduction of acetic acid.

Selectivity in the gas phase. Figure 4(B) shows the selectivity for gas products over the 5% Ni_2P/HZSM-5 catalyst at different temperatures and pressures. Gases obtained were CO, CH_4, CO_2, C_2H_4, C_2H_6, C_3H_6 and C_3H_8. At 350 °C, similar values were observed under the two different pressures, and the highest selectivities for CO (44%) and CH_4 (33%) were obtained under 2.0 MPa. The lower values of the selectivity of CO, CH_4 and C_2H_6 were attained at 400 °C and 450 °C compared to those obtained at 350 °C. At 400 °C and 450 °C, the results also demonstrated a higher selectivity of gaseous olefins (C_2H_4 and C_3H_6) compared to 350 °C. C_2H_4 and C_3H_6 are derived from the direct deoxygenation and hydrogenation of acetaldehyde and acetone over the acid sites of the HZSM-5 support, and are favored by high temperature. Significant amounts of CO and CO_2 were released because of the cracking of either carbonyl (RR′CO) or carboxyl (RCO_2H) functional groups [41]. The further hydrogenation of C_2H_4 and C_3H_6 can lead to C_2H_6 and C_3H_8.

3.2.2. *Proposed reaction pathways for acetic acid HDO*

Based on the literature [38,39,42] and products formed, a set of reaction pathways for the HDO of acetic acid is proposed in Table 2. Reaction (1) is an acetic acid direct self-ketonization and decarboxylation reaction on a coordinatively unsaturated metal site of catalyst to a ketene ($R_2C{=}C{=}O$) intermediate, and then to form acetone, CO_2 and H_2O [43]. Acetone is subsequently hydrogenated and dehydrated to C_3H_6 over the acidic function HZSM-5 in reaction (2) [44]. Reaction (3) corresponds to the reduction of acetic acid to acetaldehyde, together with the formation of H_2O. Reaction (4) is a hydrogenation/dehydration reaction of acetaldehyde produced by the reaction (3), forming C_2H_4 and H_2O. Reaction (5) is an aldol condensation reaction of acetone molecule to produce diacetone alcohol and MO intermediates followed by dehydration to form MIK [35,39]. Mesitylene can be formed by further aldol condensation between MO and acetone molecules followed by dehydration in reaction (6). Mesitylene can be further converted to other aromatic hydrocarbons via demethylation and/or alkyl substitution, such as BTX (benzene, toluene and xylene) and ethylbenzene. Reaction (7) is the main hydrogenated reaction to form propane.

3.3. *HDO of 4-ethylguaiacol*

3.3.1. *Effect of temperature and pressure*

Conversion rate, DOD, and yield. Table 3 illustrates the influence of temperature and pressure on the conversion rate of 4-ethylguaiacol, DOD, and yield of products for HDO of 4-ethylguaiacol. The evolution of the conversion rate of 4-ethylguaiacol and DOD showed a small improvement when the temperature increased from 300 °C to 500 °C. At 400 °C, a significant increase of the conversion rate (84%) and DOD (51%) under 3.0 MPa was obtained compared to 0.5 MPa, demonstrating that pressure had a greater effect on the conversion rate and DOD than temperature.

The yield of gas products and the amount of H_2O exhibited an increasing trend as the temperature increased. This can be attributed to an increase of the direct deethylation of 4-ethylguaiacol to form C_2H_6, C–O bond cleavage of the methoxy group for producing CH_4, and further dehydroxylation of phenol intermediates to give H_2O. The highest yield of 32% for gas products and of 14% for H_2O was accompanied by the lowest yield of liquid products (50%, H_2O free) at 500 °C.

In addition, a notable amount of coke (4%) was formed at 500 °C, although no coke formation was observed at lower temperatures (300 °C and 400 °C). It is clear that coke formation is favored at a high temperature, probably via the condensation of 4-ethylguaiacol during the demethoxylation reaction. In another study, Gayubo *et al.* [45] found a notable coke formation from the upgrading of 2-methoxyphenol over ZSM-5 at high temperature.

Selectivity in the liquid phase. *BTX selectivity.* Figure 5(A) shows the selectivity values of major products of 4-ethylguaiacol HDO as a function of temperature and pressure. The detail of the chemicals in the liquid products can be seen in the Supplementary materials (Table S3). The results revealed that the Ni_2P catalyzed the HDO of 4-ethylguaiacol to

Table 2. Proposed reaction pathways of HDO of acetic acid

Main products	Main reaction pathways	
Acetone	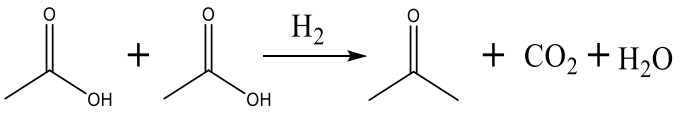	(1)
	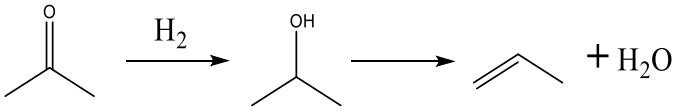	(2)
Acetaldehyde	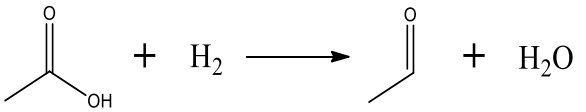	(3)
Ethylene	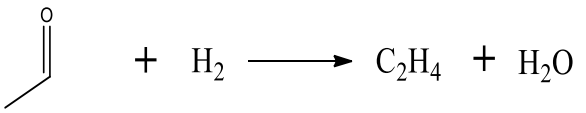	(4)
Methyl isobutyl ketone	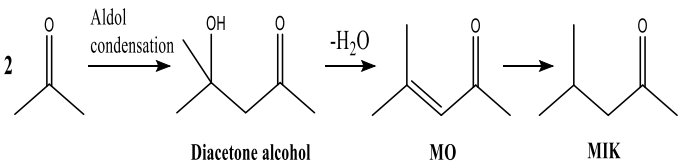	(5)
Mesitylene	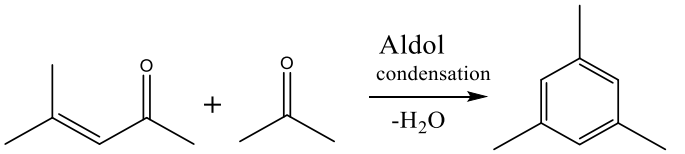	(6)
Propane	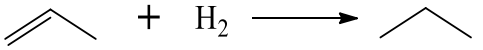	(7)

Table 3. Effect of temperature and pressure on 4-ethylguaiacol HDO

Item	Conditions[a]			
	3 MPa 300 °C	3 MPa 400 °C	3 MPa 500 °C	0.5 MPa 400 °C
Conversion rate & DOD (wt%)				
$X_{4-\text{Ethylguaiacol}}$	75	84	83	44
DOD	43	51	53	25
Yield of products (wt%)				
$Y_{\text{Liq. (free water)}}$	79	71	50	87
Y_{Gas}	12	20	32	8
Y_{H_2O}	9	9	14	5
Y_{Coke}	-	-	4	-

[a] Fixed conditions: 0.43 g 5% Ni_2P/HZSM-5 catalyst, 0.05 mL/min of 4-ethylguaiacol, H_2: 40 mL/min, N_2: 10 mL/min, 90 min.

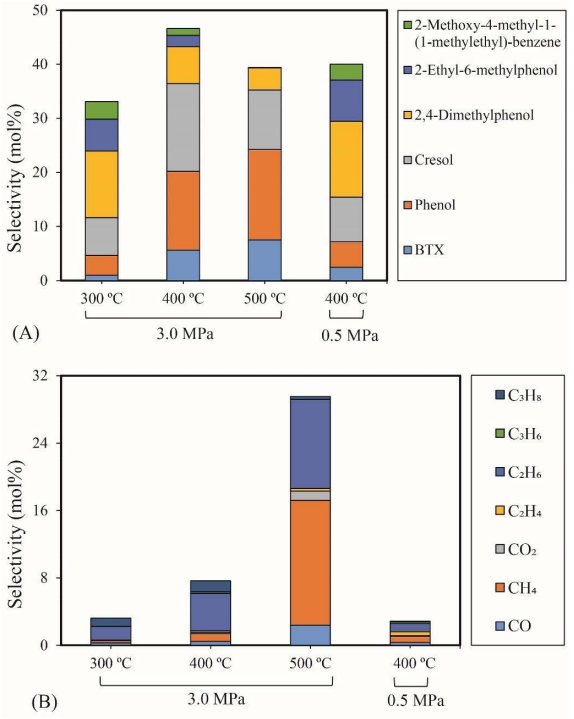

Figure 5. The influence of temperature and pressure on 4-ethylguaiacol HDO (0.43 g 5% Ni_2P/HZSM-5, 0.05 mL/min 4-ethylguaiacol, 40 mL/min H_2, 10 mL/min N_2, reaction time: 90 min): (A) Selectivity of major liquid products; (B) Selectivity of gas products.

produce oxygen-free aromatic hydrocarbons (benzene, toluene, xylene, etc.), mono-oxygenated aromatics (phenol, cresol (o- & p-), 2,4-dimethylphenol (DMP), etc.). At 300 °C, selectivities of 12% for DMP and 3% for 2-methoxy-4-methyl-1-(1-methylethyl)-benzene (MMMEB) were obtained under 3 MPa. The results under 3 MPa showed that the selectivity of MMMEB and DMP decreased when the temperature increased from 300 °C to 500 °C. This suggested that 4-ethylguaiacol was first converted to DMP via deethylation and methoxy removal, followed by alkylation/transalkylation, and the MMMEB was formed by dehydroxylation, alkylation/transalkylation and/or isomerization of 4-ethylguaiacol. These reaction pathways can be explained by the presence of a Lewis basic benzene ring of guaiacol molecules, which should be chemisorbed on Lewis acidic Ni sites of Ni_2P phase at the outset of the reaction, and then be transformed into derivatives [46]. In particular, the outset reactions needed active H species to cleave $C_{aromatic}$-OCH_3 bonds since the PO-H groups on Ni_2P phase allowed spillover of the H species to the chemisorbed guaiacol on the Ni sites of Ni_2P [31], and then further transalkylation occurred on Brønsted acid sites [47].

Cresol selectivity. In particular, the selectivity of cresol first increased and then decreased as the temperature increased. In addition, the selectivity of phenol and BTX increased as the temperature rose. These results can be explained by the fact that the initial increase of cresol is due to the demethylation of DMP, and subsequent decrease to further demethylation and/or dehydroxylation to form phenol and aromatic hydrocarbons. High temperature favored C–C and C–O bond cleavage between the aromatic ring and its branched chains. The highest selectivity of cresol (16%) was obtained at 400 °C and 3 MPa.

MMMEB selectivity. At 400 °C and under 0.5 MPa, it was observed that the selectivity of MMMEB (3%) and DMP (14%) was higher than that obtained under 3 MPa, while the selectivity of cresol (8%), phenol (5%) and BTX (2%) decreased significantly. It is therefore clear that high pressure favored the further reaction of MMMEB and DMP to form cresol, phenol and BTX. Subsequently, cresol and phenol underwent dehydroxylation and/or demethylation to produce BTX. Other phenols identified in the liquid phase, such as 3-methyl-4-isopropylphenol and 2-ethyl-6-methylphenol, are probably produced via the isomerization of reaction intermediates. Notably, the selectivity of 2-ethyl-6-methylphenol first decreased due to a further dealkylation and then increased due to coke formation. Probably, the coke affected the pore size of the catalysts, which suppressed further dealkylation.

Selectivity in the gas phase. ***Gas products selectivity.*** Figure 5(B) shows the evolution of the selectivity of gas products for 4-ethylguaiacol HDO over the 5% Ni_2P/HZSM-5 catalyst at different temperatures and pressures. As can be seen, the selectivity of gas products increased with the increase of temperature. The main gas product was C_2H_6 at 300 °C and 400 °C, followed by C_3H_8 or CH_4. At 500 °C, CH_4 and C_2H_6 were the major products in gas phase. C_2H_6 can be produced via deethylation of 4-ethylguaiacol followed by

hydrogenation. CH_4 can be formed via various reaction routes, mainly via methoxy removal from 4-ethylguaiacol followed by further C–O bond to give some CO and, to a lesser extent, via direct demethylation of cresol intermediate.

The increase in selectivity of CH_4 and C_2H_6 revealed that high temperature promotes C–O bond cracking of the methoxy group and multiple C–C hydrogenolysis of 4-ethylguaiacol and other intermediates. Chen *et al.* [48] found that methane was yielded as a main gas product in the hydrogenation of m-cresol via C–C bond cleavage on silica supported Ni catalyst. The highest selectivity of C_2H_6 (11%) and CH_4 (15%) was obtained at 500 °C. Under 3 MPa, a significant increase in the selectivity of total gas products was observed and particularly C_2H_6 and C_3H_8. This behavior proves that higher pressure improved the HDO of 4-ethylguaiacol to form gas products and especially favored C_2H_6 and C_3H_8. This last was possibly formed by an addition reaction between CH_4 and C_2H_4.

3.3.2. *Proposed reaction pathways of 4-ethylguaiacol HDO*

Based on the products formed, and the discussion in Section 3.2.1, a set of reaction pathways for the HDO of 4-ethylguaiacol is proposed and reported in Table 4. Reaction (1) corresponds to the dealkylation of 4-ethylguaiacol to 2-methoxyphenol and demethoxylation to 4-ethylphenol on Lewis acidic Ni sites, with the formation of C_2H_4, CH_4 and H_2O. The C_2H_4 was then hydrogenated to C_2H_6. Reaction (2) is a direct demethoxylation and alkylation reaction of 4-ethylguaiacol forming DMP below 400 °C. This is a key reaction because DMP is the most primary product at 300 °C. Reaction (3) is a dihydroxylation and alkylation reaction of 4-ethylguaiacol to form MMMEB at 300 °C and 400 °C. Instead of the alkylation reaction favored by relatively low temperatures, the dealkylation reaction, namely, the C–C bond breakage between benzene ring and its side alkyl group, was promoted by high temperatures. The DMP underwent subsequent demethylation to form cresol (p- & o-) and phenol in reaction (4). Reaction (5) is a dealkylation reaction of cresol to produce phenol and CH_4. Similarly, phenol and CH_4 were also identified as important products of guaiacol HDO [20,49]. Aromatic hydrocarbons can be formed by the further dehydration reaction of alkylphenols, as shown in reactions (6) and (7). Other alkylphenols, (3-methyl-4-isopropylphenol, for example), were probably produced via the isomerization of certain intermediates.

3.4. *HDO of furfural*

3.4.1. *Effect of temperature and pressure*

Conversion rate, DOD, and yield. Table 5 presents the effect of temperature and pressure on the conversion rate, DOD, and yield of products for furfural HDO. Results under 3 MPa pressure exhibited a significant increase in conversion rate (from 54% to 100%) and DOD (from 39% to 92%) when the temperature increased from 300 °C to 500 °C. The highest yields of gas products (51%) and H_2O (10%) were obtained at 500 °C and 3 MPa and were accompanied by the lowest yield of liquid products (39%, H_2O free). At 400 °C and 3 MPa, the results showed a slight increase of the conversion rate and a decrease of liquid products and H_2O compared to the results under 0.5 MPa. These results indicated that high pressure promoted the C–C hydrogenolysis between the furan ring and its branched chains and reduced the direct dehydration reaction to some extent.

Selectivity in the liquid phase. The selectivity of major products of furfural HDO is illustrated in Figure 6(A). The detailed chemical composition of products can be found in the Supplementary (Table S4). Generally, high selectivities of furan, 2-methylfuran (2-MF), butanal, BTXM, and 1-methylindan were observed in these conditions.

Furan selectivity. Furan was observed as the most primary product of furfural HDO, with the selectivity of 17% (300 °C and 3 MPa), 22% (400 °C and 3 MPa) and 17% (400 °C and 0.5 MPa). It can be deduced that direct aldehyde removal was the main reaction of furfural HDO in these conditions, and this removal was promoted by the pressure increase. Furthermore, deoxygenation of the aldehyde group of furfural under 3 MPa was also a significant reaction, since high selectivities of 2-MF (17% and 10%) were achieved at 300 °C and 400 °C. Accordingly, these results proved that the high pressure favored the aldehyde removal and deoxygenation of furfural but less furan ring-opening on the acid sites of 5% Ni_2P/HZSM-5

Table 4. The proposed HDO pathways of 4-ethylguaiacol

Main products	Main reaction pathways	
4-Ethylphenol & 2-methoxyphenol	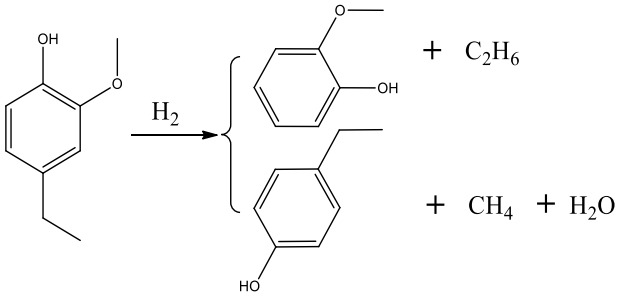	(1)
DMP	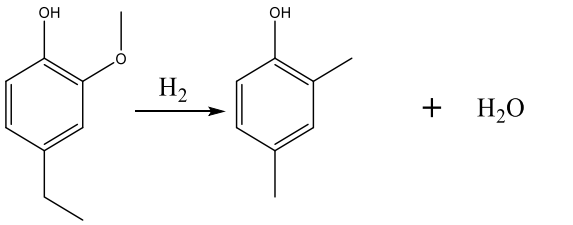	(2)
MMMEB	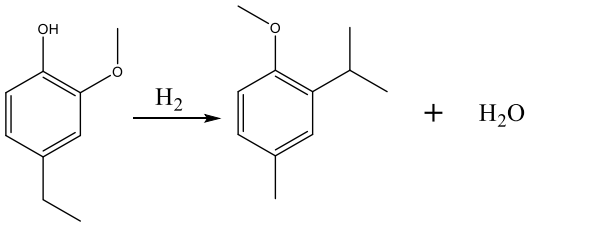	(3)
Cresol (o- & p-) & Phenol	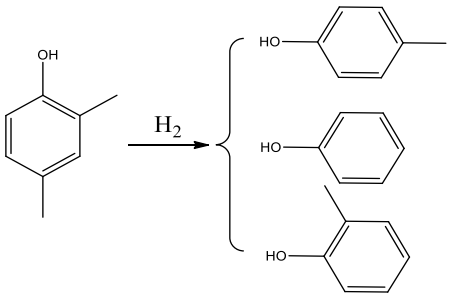	(4)
Phenol	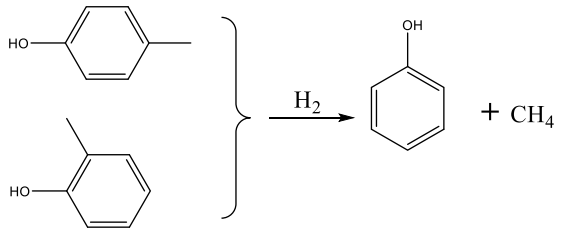	(5)

(continued on next page)

Table 4. (continued)

Main products	Main reaction pathways	
Benzene	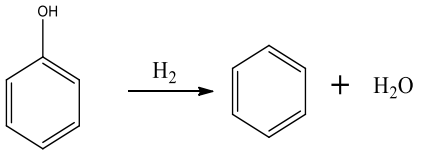	(6)
Toluene & Xylene (p- & m-)	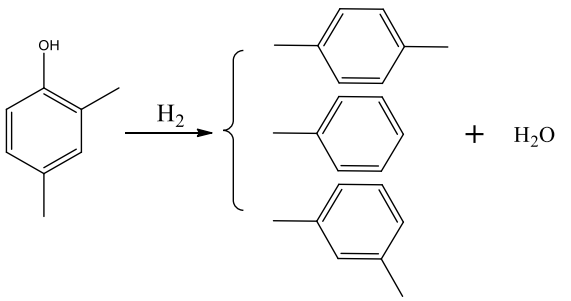	(7)

Table 5. Effect of temperature and pressure on furfural HDO

Item	Conditions[a]			
	3 MPa 300 °C	3 MPa 400 °C	3 MPa 500 °C	0.5 MPa 400 °C
Conversion rate & DOD (wt%)				
X_{Furfural}	54	66	100	57
DOD	39	51	92	35
Yield of products (wt%)				
$Y_{\text{Liq. (free water)}}$	75	64	39	65
Y_{Gas}	19	28	51	26
Y_{H_2O}	6	8	10	9

[a] Fixed conditions: 0.43 g 5% Ni_2P/HZSM-5 catalyst, 0.05 mL/min of furfural, H_2: 40 mL/min, N_2: 10 mL/min, 90 min.

catalyst. Similarly, Cai *et al.* [50] reported that HDO reactions of furfural mainly happened on its aldehyde group, but little on furan ring using Cu/SiO_2 catalyst. At 500 °C, a very low selectivity of furan was obtained demonstrating that temperature promoted the cracking of furan.

BTXM and 1-methylindan selectivities. A greater amount of BTXM was obtained at higher temperatures of 400 °C and 500 °C than at 300 °C. In this case, the formation of aromatic hydrocarbons can be attributed to the oligomerization of mono-olefins (C_2H_4, C_3H_6 and C_4H_8) and/or dienes followed by cyclization at high temperatures. Under 3 MPa, the selectivity of BTXM (6%) at 500 °C decreased slightly compared to the value of 10% at 400 °C, probably due to the further oligomerization reaction of BTXM and olefins to 1-methylindan with a high selectivity of 1-methylindan (21%). The various olefins can be produced by the ring-opening reaction of furan, 2-methylfuran and other intermediate reactions. In the literature, Cai *et al.* also mentioned the role of oligomerization and cyclization of olefins to produce aromatic hydrocarbons [50].

2-vinylfuran selectivity. A small amount of 2-vinylfuran was detected, which might be linked to a route of direct substitution reaction between furan and C_2H_4. Although, 2-vinylfuran was observed as a secondary product in the case of hydrotreatment of the furfural–acetone condensation reaction by Ulfa *et al.* [51] and the catalytic reduction of furfural–methanol by Grazia *et al.* [52], a few studies reported that 2-vinylfuran was a product of furfural hydrotreatment without other co-reagents. The 2-vinylfuran can potentially be obtained from the methylenation reaction of furfural involving several consolidating approaches. The most frequently used methods for furfural conversion reaction are the Wittig [53] and Horner–Wadsworth–Emmons reactions [54], which have the common feature of employing the co-reagent of phosphorus-substituted carbanions. One can then suggest that the active Ni_2P phase of the Ni_2P/HZSM-5 catalyst favored the olefin substitution reaction of furan via the interaction between Ni_2P and ethylene.

Other compounds. At low temperature, the formation of butanal can be attributed to the ring-opening reaction and further hydrogenation of furan. The acetone was possibly produced via the ring-opening reaction of 2-MF followed by the further hydrogenolysis reaction of C–C bond together with the release of C_2H_4.

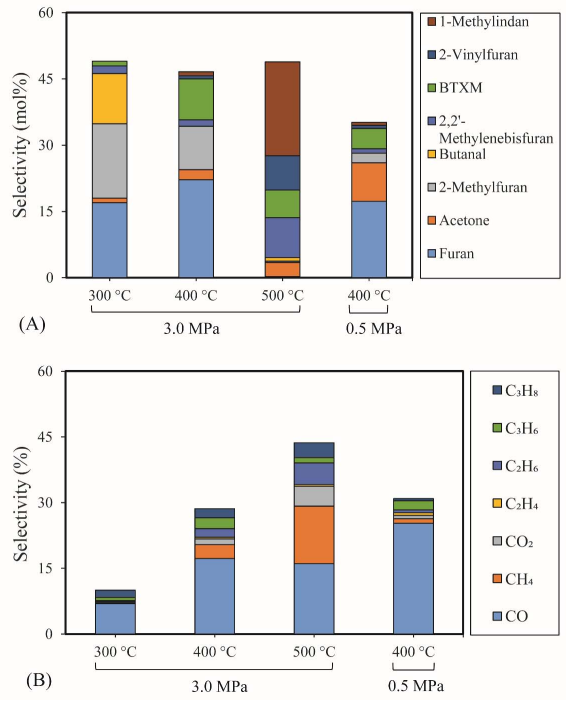

Figure 6. The influence of temperature and pressure on furfural HDO (0.43 g 5% Ni_2P/HZSM-5, 0.05 mL/min furfural, 40 mL/min H_2, 10 mL/min N_2, reaction time: 90 min): (A) Selectivity of major liquid products; (B) Selectivity of gas products.

Selectivity in the gas phase. Figure 6(B) shows the analysis of various gas products during the furfural HDO reaction. The results showed a very low gas production at 300 °C due to the low conversion rate of furfural at low temperatures. The main gas product was CO with a selectivity of 17%. High selectivity of other gases (CH_4, CO_2, C_2H_6, C_3H_6 and C_3H_8) at 400 °C and 3 MPa was also observed. CO was mainly formed by the direct decarbonylation of furfural and aldehyde intermediates (like butanal). CO_2 was possibly produced by the 2-MF ring-opening reaction followed by C–C bond cracking at high temperatures.

Among these gaseous products, light alkanes were formed by the hydrogenation reaction of intermediates of furfural HDO since the ring-opening reaction produced olefins. Notably, the selectivity of CH_4 (13%) at 500 °C is significantly higher than at 400 °C, but the selectivity of CO was lower compared to 400 °C. CH_4 can be formed mainly by the demethylation of 2-MF and probably by hydrogenation of CO and CO_2, as reported in the literature in the case of metal Ni under high pressure of H_2 [55]. These results suggested that the selectivity of alkanes depends on the relative rates of the C–C bond cleavage, dehydration and hydrogenation reactions of furfural and its intermediates. Similarly, Davda *et al.* also stated that the selectivity of various alkanes is strongly linked to the relative rates of the C–C bond cleavage, dehydration and hydrogenation reactions during the aqueous-phase processing of sorbitol [55]. At 400 °C, the gas product selectivity under 0.5 MPa showed a relatively narrow distribution compared to 3 MPa, and CO was the most important product, with 25% of selectivity. Thus, it can be deduced that pressure had a significant effect on the distribution of gas products of furfural HDO and that high pressure facilitated the ring-opening reactions.

Table 6. The proposed HDO pathways of furfural

Main products	Main reaction pathways	
2-Methylfuran	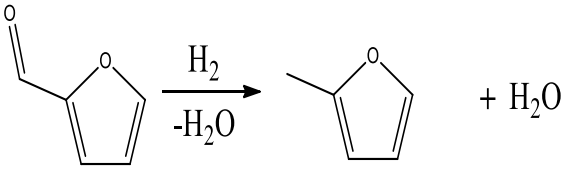	(1)
Furan & CO	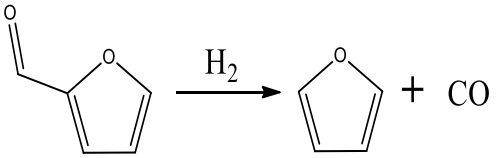	(2)
	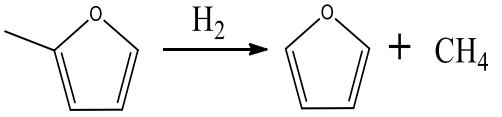	(3)
Acetone	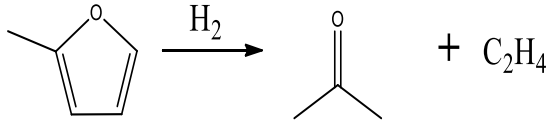	(4)
Butanal & C_4H_8	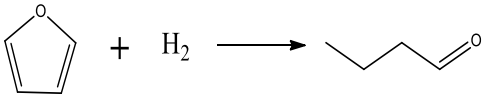	(5)
	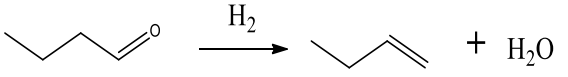	(6)
C_3H_6 & C_3H_8	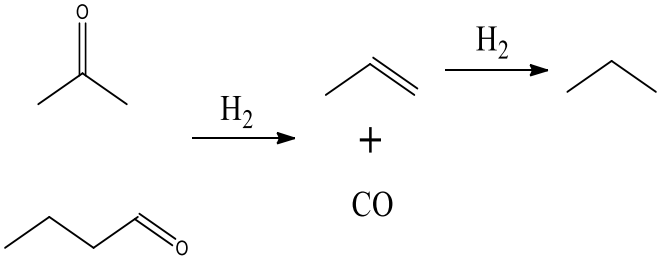	(7)
2-Vinylfuran	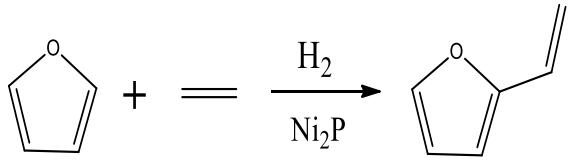	(8)

(continued on next page)

Table 6. (continued)

Main products	Main reaction pathways	
2,2-Methylenebisfuran	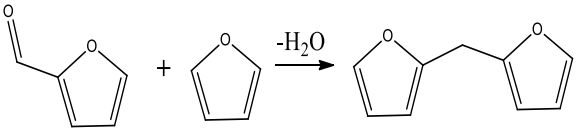	(9)
Aromatic hydrocarbons	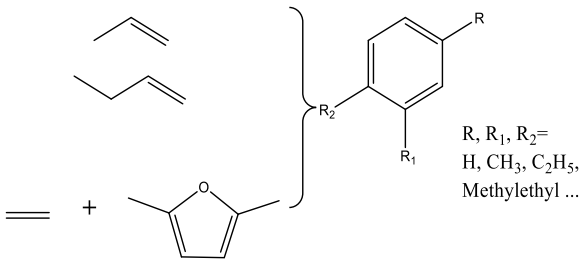	(10)

3.4.2. *Proposed reaction pathways of furfural HDO*

Table 6 summarizes a series of reaction pathways for the HDO of furfural according to the main products obtained. Reaction (1) corresponds to the hydrodehydration of furfural to 2-MF, together with the formation of H_2O. Reaction (2) is a direct decarbonylation reaction of furfural forming furan and CO [56]. This reaction is the primary route of furan formation due to the highest selectivity of CO among other gas products (Figure 6B). Reaction (3) can be considered a minor reaction for furan production, associated with the formation of CH_4. Acetone was produced by the ring-opening reaction of 2-methylfuran accompanying the release of C_2H_4 in reaction (4). C_3H_6 and C_3H_8 can be produced mainly from the dehydration–hydrogenation of acetone in reaction (7), and C_2H_4 can be easily converted to C_2H_6 by hydrogenation.

Furan can be converted by hydro-opening-ring and hydrogenation to form butanal in reaction (5). Subsequently, butanal can be hydrogenated, and then dehydrated forming C_4H_8 in reaction (6) and/or directly decarbonylated to form CO and C_3H_6. C_3H_8 is then formed by hydrogenation of C_3H_6 in reaction (7). Reaction (8) is the probable pathway allowing the formation of 2-vinylfuran from furan and C_2H_4. Reaction (9) is a condensation reaction between furfural and furan molecules to synthesize the 2,2-methylenebisfuran. Reaction (10) is a probable route of aromatic hydrocarbons via the addition reaction of olefins on Ni_2P and subsequent cyclization on HZSM-5 acidic sites. As stated in the literature, aromatic hydrocarbons can be formed by cyclization–dehydration of dienes, which comes from the oligomerization of mono-olefins (C_2H_4, C_3H_6 and C_4H_8) [50] or the Diels–Alder cycloaddition of 2,5-dimethylfuran with ethylene and subsequent dehydration to form p-xylene, followed by alkylation to other aromatics [57,58]. Thus, it can be deduced that 1-methylindan was also formed by these routes.

4. Conclusion

The HDO of acetic acid, 4-ethylguaiacol, and furfural as model molecules of bio-oil with the use of prepared Ni_2P/HZSM-5 catalysts was studied, which could provide significant guidance for the upgrading of crude bio-oil. The results showed that the reaction temperature has a pronounced effect on the conversion rate and DOD of acetic acid and furfural using 5% Ni_2P/HZSM-5 catalyst. However, pressure had a greater effect on the conversion rate and DOD of 4-ethylguaiacol HDO than temperature.

For acetic acid HDO, the temperature and pressure mainly affected the decarboxylation, hydrogenation, and further decarbonylation associated with the release of CO, CH_4, and CO_2. Aromatic hydrocarbons were obtained via a further aldol condensation between MIK and acetone molecules followed by dehydration and hydrogenation.

The results of 4-ethylguaiacol HDO illustrated that 2,4-dimethylphenol, cresol, and 2-ethyl-6-methylphenol were the most important reaction intermediates. The final products, such as phenol and BTX (benzene, toluene, and xylene), can be produced from those intermediates via dealkylation, dehydroxylation and isomerization. Notably, the coke formation had a slight effect on the conversion rate of 4-ethylguaiacol, but significantly affected the further dealkylation of the 2-ethyl-6-methylphenol intermediate.

Moreover, it was proved that the principal reaction of furfural HDO was the direct decarbonylation with furan and CO formation. Higher temperatures and pressures promoted the ring-opening reaction and C–C hydrogenolysis of furfural HDO. Aromatic hydrocarbons from furfural HDO were probably formed by the addition reaction and subsequent cyclization–dehydration of dienes, which come from the oligomerization of mono-olefins during the ring-opening and C–C bond cleavage process.

Abbreviations

HDO	Hydro-deoxygenation
DMP	2,4-Dimethylphenol
MO	Mesityl oxide
MIK	Methyl isobutyl ketone
BTX	Benzene, Toluene and Xylene
BTXM	Benzene, Toluene, Xylene and Mesitylene
2-MF	2-Methylfuran
DOD	Degree of deoxygenation
BET	Brunauer–Emmett–Teller
XRD	X-ray Powder Diffraction
TPR	Temperature-programmed reduction
ICP-OES	Inductively Coupled Plasma-Optical Emission Spectrometry
FT-IR	Fourier Transform Infrared Spectroscopy
DSC	Differential Scanning Calorimeter
X (%)	Conversion rate
Sel_i (%)	The selectivity of product chemicals
Y_i (%)	The yield of products
W (%)	Water content

Conflicts of interest

There are no conflicts of interests to declare.

Acknowledgments

This work was supported by China Scholarship Council (CSC) and UT-INSA program between China and France. The authors give great thanks to the GenComm Interreg project that offered the opportunity for the internship in this work.

Supplementary data

Supporting information for this article is available on the journal's website under https://doi.org/10.5802/crchim.122 or from the author.

References

[1] W. N. R. W. Isahak, M. W. M. Hisham, M. A. Yarmo, T. Yun Hin, *Renew. Sustain. Energy Rev.*, 2012, **16**, 5910-5923.
[2] F. Abnisa, W. M. A. Wan Daud, A. Arami-Niya, B. S. Ali, J. N. Sahu, *Energy Fuels*, 2014, **28**, 3074-3085.
[3] H. Jahromi, F. A. Agblevor, *Ind. Eng. Chem. Res.*, 2018, **57**, 13257-13268.
[4] N. Boukaous, L. Abdelouahed, M. Chikhi, C. Mohabeer, A. H. Meniai, B. Taouk, *C. R. Chim.*, 2020, **23**, 623-634.
[5] N. Koike, S. Hosokai, A. Takagaki, S. Nishimura, R. Kikuchi, K. Ebitani, Y. Suzuki, S. T. Oyama, *J. Catal.*, 2016, **333**, 115-126.
[6] J. Xu, J. Jiang, J. Chen, Y. Sun, *Bioresour. Technol.*, 2010, **101**, 5586-5591.
[7] T. N. Pham, D. Shi, D. E. Resasco, *Adv. Catal. Biomass Valorization*, 2014, **145**, 10-23.
[8] H. Hammani, M. E. Achaby, K. E. Harfi, M. A. E. Mhammedi, A. Aboulkas, *C. R. Chim.*, 2020, **23**, 589-606.
[9] B. Valle, A. Remiro, N. García-Gómez, A. G. Gayubo, J. Bilbao, *J. Chem. Technol. Biotechnol.*, 2019, **94**, 670-689.
[10] A. Infantes-Molina, E. Gralberg, J. A. Cecilia, E. Finocchio, E. Rodríguez-Castellón, *Catal. Sci. Technol.*, 2015, **5**, 3403-3415.
[11] P. Zhang, Y. Sun, M. Lu, J. Zhu, M. Li, Y. Shan, J. Shen, C. Song, *Energy Fuels*, 2019, **33**, 7696-7704.
[12] Y. Han, M. Gholizadeh, C.-C. Tran, S. Kaliaguine, C.-Z. Li, M. Olarte, M. Garcia-Perez, *Fuel Process. Technol.*, 2019, **195**, article no. 106140.
[13] A. Berenguer, T. M. Sankaranarayanan, G. Gómez, I. Moreno, J. M. Coronado, P. Pizarro, D. P. Serrano, *Green Chem.*, 2016, **18**, 1938-1951.
[14] S. Gutiérrez-Rubio, I. Moreno, D. P. Serrano, J. M. Coronado, *ACS Omega*, 2019, **4**, 21516-21528.
[15] M. R. Shabani, M. A. Moosavian, Y. Zamani, S. J. Royaee, *C. R. Chim.*, 2020, **23**, 433-444.
[16] H. Shi, J. Chen, Y. Yang, S. Tian, *Fuel Process. Technol.*, 2014, **118**, 161-170.
[17] A. Berenguer, S. Gutiérrez-Rubio, M. Linares, C. Ochoa-Hernández, I. Moreno, J. L. García-Fierro, J. M. Coronado, D. P. Serrano, P. Pizarro, *Energy Technol.*, 2019, **7**, article no. 1900214.
[18] B. S. Chen, J. L. Falconer, *J. Catal.*, 1994, **147**, 72-81.

[19] B. Peng, C. Zhao, S. Kasakov, S. Foraita, J. A. Lercher, *Catal. Chem.–Eur. J.*, 2013, **19**, 4732-4741.
[20] F. Broglia, L. Rimoldi, D. Meroni, S. De Vecchi, M. Morbidelli, S. Ardizzone, *Fuel*, 2019, **243**, 501-508.
[21] S. T. Oyama, T. Onkawa, A. Takagaki, R. Kikuchi, S. Hosokai, Y. Suzuki, K. K. Bando, *Top. Catal.*, 2015, **58**, 201-210.
[22] W. Li, H. Wang, X. Wu, L. E. Betancourt, C. Tu, M. Liao, X. Cui, F. Li, J. Zheng, R. Li, *Fuel*, 2020, **274**, article no. 117859.
[23] Q. K. Tran, H. V. Ly, B. Kwon, S.-S. Kim, J. Kim, *Renew. Energy.*, 2021, **173**, 886-895.
[24] E. Laurent, A. Centeno, B. Delmon, "Coke formation during the hydrotreating of biomass pyrolysis oils: influence of guaiacol type compounds", in *Catalyst Deactivation* (B. Delmon, G. F. Froment, eds.), Stud. Surf. Sci. Catal., vol. 88, Elsevier, Ostend, Belgium, 1994, 573-578.
[25] X. Zhang, T. Wang, L. Ma, C. Wu, *Fuel*, 2010, **89**, 2697-2702.
[26] C. Zhao, J. A. Lercher, *Angew. Chem. Int. Ed.*, 2012, **51**, 5935-5940.
[27] Z. Wang, Z. Fu, W. Lin, S. Li, W. Song, *Korean J. Chem. Eng.*, 2019, **36**, 1235-1242.
[28] X. Lan, R. Pestman, E. J. M. Hensen, T. Weber, *J. Catal.*, 2021.
[29] C. Mohabeer, L. Abdelouahed, S. Marcotte, B. Taouk, *J. Anal. Appl. Pyrolysis*, 2017, **127**, 269-277.
[30] J. Wang, M. Jabbour, L. Abdelouahed, S. Mezghich, L. Estel, K. Thomas, B. Taouk, *Can. J. Chem. Eng.*, 2021, **99**, 1082-1093.
[31] S.-K. Wu, P.-C. Lai, Y.-C. Lin, *Catal. Lett.*, 2014, **144**, 878-889.
[32] M. Eddaoudi, *J. Am. Chem. Soc.*, 2005, **127**, article no. 14117.
[33] J. Chen, L. Sun, R. Wang, J. Zhang, *Catal. Lett.*, 2009, **133**, article no. 346.
[34] A. C. Badari, S. Harnos, F. Lónyi, G. Onyestyák, M. Štolcová, A. Kaszonyi, J. Valyon, *Catal. Commun.*, 2015, **58**, 1-5.
[35] S. K. Bej, L. T. Thompson, *Appl. Catal. Gen.*, 2004, **264**, 141-150.
[36] J. J. Gamman, S. D. Jackson, F. A. Wigzell, *Ind. Eng. Chem. Res.*, 2010, **49**, 8439-8443.
[37] A. A. Nikolopoulos, B. W.-L. Jang, J. J. Spivey, *Appl. Catal. Gen.*, 2005, **296**, 128-136.
[38] X. Huo, N. A. Huq, J. Stunkel, N. S. Cleveland, A. K. Starace, A. E. Settle, A. M. York, R. S. Nelson, D. G. Brandner, L. Fouts, P. C. St. John, E. D. Christensen, J. Luecke, J. H. Mack, C. S. McEnally, P. A. Cherry, L. D. Pfefferle, T. J. Strathmann, D. Salvachúa, S. Kim, R. L. McCormick, G. T. Beckham, D. R. Vardon, *Green Chem.*, 2019, **21**, 5813-5827.
[39] W. Zhang, Y. Zhang, L. Zhao, W. Wei, *Energy Fuels*, 2010, **24**, 2052-2059.
[40] J. Wang, M. Jabbour, L. Abdelouahed, S. Mezghich, L. Estel, K. Thomas, B. Taouk, *Can. J. Chem. Eng.*, 2021, **99**, 1082-1093.
[41] H. Zhang, R. Xiao, B. Jin, G. Xiao, R. Chen, *Bioresour. Technol.*, 2013, **140**, 256-262.
[42] I. L. Simakova, D. Y. Murzin, *J. Energy Chem.*, 2016, **25**, 208-224.
[43] T. N. Pham, T. Sooknoi, S. P. Crossley, D. E. Resasco, *ACS Catal.*, 2013, **3**, 2456-2473.
[44] A. Witsuthammakul, T. Sooknoi, *Catal. Sci. Technol.*, 2016, **6**, 1737-1745.
[45] A. G. Gayubo, A. T. Aguayo, A. Atutxa, R. Aguado, J. Bilbao, *Ind. Eng. Chem. Res.*, 2004, **43**, 2610-2618.
[46] M. Xue, S. Hu, H. Chen, Y. Fu, J. Shen, *Catal. Commun.*, 2011, **12**, 332-336.
[47] X. Zhu, L. L. Lobban, R. G. Mallinson, D. E. Resasco, *J. Catal.*, 2011, **281**, 21-29.
[48] C. Chen, G. Chen, F. Yang, H. Wang, J. Han, Q. Ge, X. Zhu, *Chem. Eng. Sci.*, 2015, **135**, 145-154.
[49] X. Lan, E. J. M. Hensen, T. Weber, *Appl. Catal. Gen.*, 2018, **550**, 57-66.
[50] Q. Cai, J. Xu, S. Zhang, S. Wang, *Ind. Eng. Chem. Res.*, 2016, **55**, 10839-10849.
[51] S. M. Ulfa, R. Munandar, D. Prihartini, *AIP Conf. Proc.*, 2018, **2049**, article no. 020005.
[52] L. Grazia, D. Bonincontro, A. Lolli, T. Tabanelli, C. Lucarelli, S. Albonetti, F. Cavani, *Green Chem.*, 2017, **19**, 4412-4422.
[53] J. Arekion, M. Delmas, A. Gaset, *Biomass*, 1983, **3**, 59-65.
[54] J. F. Reichwein, B. L. Pagenkopf, *J. Am. Chem. Soc.*, 2003, **125**, 1821-1824.
[55] R. R. Davda, J. W. Shabaker, G. W. Huber, R. D. Cortright, J. A. Dumesic, *Appl. Catal. B*, 2003, **43**, 13-26.
[56] S. K. Jaatinen, R. S. Karinen, J. S. Lehtonen, *ChemistrySelect.*, 2017, **2**, 51-60.
[57] C. L. Williams, C.-C. Chang, P. Do, N. Nikbin, S. Caratzoulas, D. G. Vlachos, R. F. Lobo, W. Fan, P. J. Dauenhauer, *ACS Catal.*, 2012, **2**, 935-939.
[58] C.-C. Chang, S. K. Green, C. L. Williams, P. J. Dauenhauer, W. Fan, *Green Chem.*, 2014, **16**, 585-588.